KINEMATIC AND DYNAMIC ANALYSIS OF AN ANTHROPOMORPHIC HAND-ARM SYSTEM

Ştefan DUMITRU[1], Andrei CRAIFALEANU[2]

The paper presents an anthropomorphic hand-arm system, designed to automatically perform common domestic tasks. An existing commercial gripper was used and improved to add functionality and reduce weight. A complete direct kinematic and dynamic analysis was performed, aimed to determine the motion of the system, the actuation torques and forces, as well as the reactions in the joints The obtained results provide useful calculation data for the basic design of a hand-arm robotic system, as well as for an optimization process.

Keywords: anthropomorphic gripper, anthropomorphic arm, underactuated.

1. Introduction

Most grippers used nowadays in the industry consist of 1 or 2 degrees of freedom (DOF) mechanisms intended for simple, repetitive operations [1].

The anthropomorphic grippers, in contrast with the industrial ones, have a more versatile gripping method and confer the possibility of manipulating an already grasped object. Therefore, they have become an increasingly interesting research subject in recent years [2], [3].

The human hand consists of 27 bones (14 phalanges, 5 metacarpals and 8 carpals), which can be modeled as a system of rigid bodies, linked through either single or double joints, creating a system with 25 DOF [4], [5].

Many anthropomorphic robotic hands with a high number of DOF can be found in the literature, such as the Gifu hand II [6] or the OCU Hand I [7], with 16 and 19 DOF, respectively. However, such mechanisms are complex and difficult to use efficiently. Therefore, to reduce the weight and complexity, gripping systems with reduced numbers of DOF can be implemented, by using mechanisms with fewer actuators and supplementary constraints, such as the HRI Hand [8], or the Alaris Hand [9], which have 6 DOF each.

The paper presents an anthropomorphic hand-arm system intended to automatically perform common domestic tasks. An existing commercial gripper, *Lobot uHand* [10], [11] (Fig. 1), was used as a model, but this model was

[1] Assist. Prof., Dept. of Mechanics, University POLITEHNICA of Bucharest, Romania, e-mail: stefan.dumitru2605@upb.ro
[2] Prof., Dept. of Mechanics, University POLITEHNICA of Bucharest, Romania, e-mail: andrei.craifaleanu@upb.ro

improved by introducing a supplementary degree of freedom to the thumb and by replacing the original servomotors with linear ones, in order to add functionality and to reduce weight. Furthermore, an arm system, conceived by the authors, was added, to achieve a complete hand-arm robot. 3D models of the modified gripper and the resulting system, respectively, created by the authors in the CATIA V5 CAD program, are presented in Figures 2-3.

The *uHand* gripper was previously studied in references [12], [13], [14], where the positions of the component elements were determined. However, a kinematic analysis, a dynamic analysis and an experimental study are not available.

The present paper goes further, by performing, for the entire hand-arm system, a kinematic study, which determines the velocity and acceleration distributions, as well as a dynamic study, which, for a given motion, calculates the necessary actuation torques and forces, as well as the reactions in the joints.

Fig. 1. The *uHand* gripper

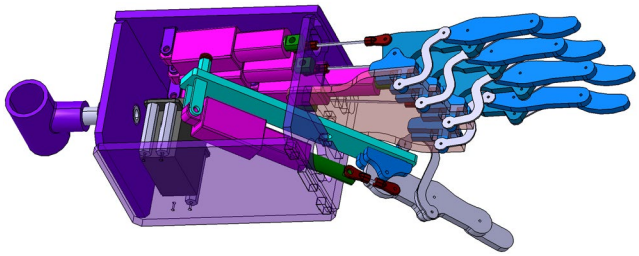

Fig. 2. 3D model of the studied gripper

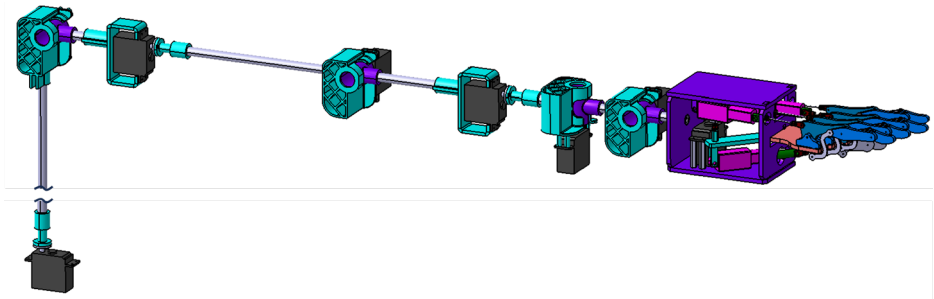

Fig. 3. 3D-model of the robotic arm

2. Model of the hand-arm system

The human arm consists of 3 joints, a spherical joint located in the shoulder and two double joints, one located in the elbow and the other in the wrist.

The spherical and double joints are difficult to construct and operate precisely, therefore they have been replaced with a series of revolute joints, which perform the same kinematic function, as can be seen in Figure 4.

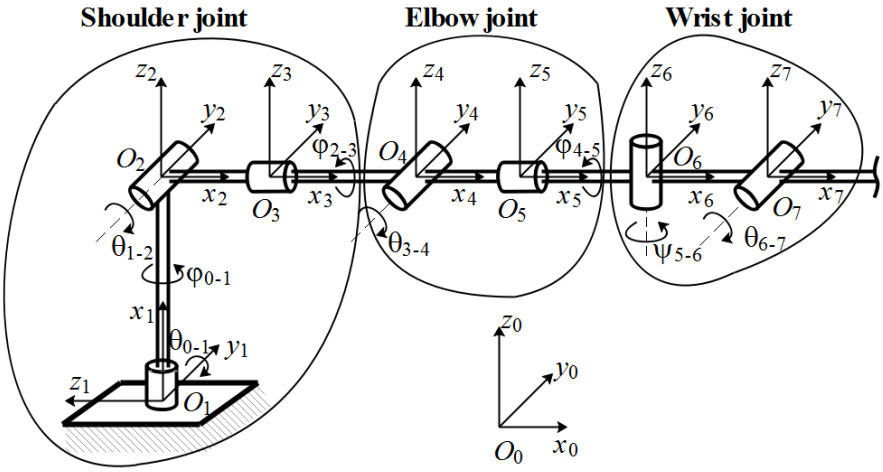

Fig. 4. Mechanical model of the anthropomorphic robotic arm

Therefore, the resultant anthropomorphic robotic arm has 7 revolute joints with 7 rotational degrees of freedom, defined by angles $\varphi_{0\text{-}1}$, $\theta_{1\text{-}2}$, $\varphi_{2\text{-}3}$, $\theta_{3\text{-}4}$, $\varphi_{4\text{-}5}$, $\psi_{5\text{-}6}$ and $\theta_{6\text{-}7}$ with respect to axes x_1, y_2, x_3, y_4, x_5, z_6 and y_7, respectively.

The reference system of each element has been positioned so that the x-axis is orientated towards the next joint in the kinematic chain. The $Ox_1y_1z_1$ coordinate system has been rotated with respect to the global coordinate system $Ox_0y_0z_0$, about the y_0 axis, with the angle $\theta_{0\text{-}1}$=-90° (Fig. 4).

The rotations about the previously described axes are performed using several servos.

The *uHand* gripper in Figure 1 is a mechanism with 5 mobilities, one for each finger, and it was modeled after a right-handed human hand. The fingers are actuated by servos. One disadvantage of an underactuated gripper, such as the *uHand* mechanism, is the inability to manipulate the grasped object with the thumb. Therefore, an extra mobility of the thumb was added (Fig. 5).

The added mobility is a rotation about an axis perpendicular to the plate on which the fingers are fixed.

For all five fingers, reference system 10 is rotated with an angle $\psi_{7\text{-}10}$ with respect to reference system 7 (Fig. 5 b). For the thumb (finger 1), this angle is

variable and it is controlled using the newly added four-bar mechanism $O_8O_9FO_{10}$, which allows the rotation of the body FO_{10}, about the axis z_{10}. For the fingers 2-5 (according to the numbering in Fig. 5 a), angle $\psi_{7\text{-}10}$ is constant and the mechanism $O_8O_9FO_{10}$ is absent, therefore in their cases, coordinate systems 8, 9 and 10 coincide.

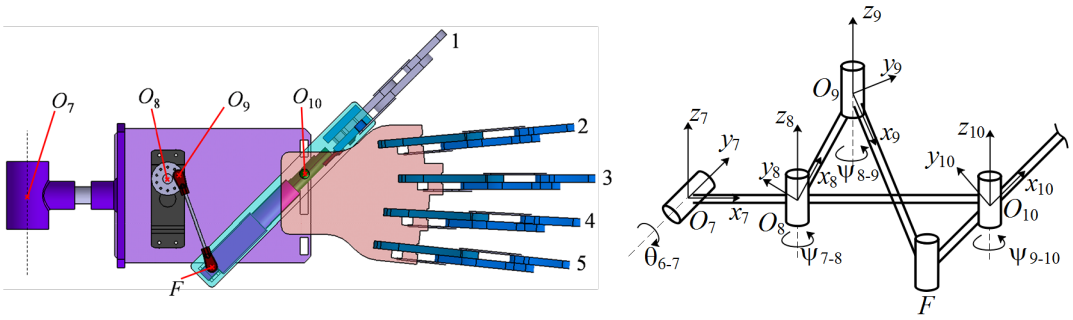

a) 3D model b) Detail of the mechanical model

Fig. 5. Extra mobility system of the thumb

All five fingers have the same mechanical structure (Fig. 6). Elements of fingers 2-5 have the same dimensions, while the elements of the thumb (finger 1) are different (see Appendix).

Each finger of the gripper is actuated by a linear motor so that the proximal phalanx has a rotational motion with respect to the O_{13} joint (Fig. 6).

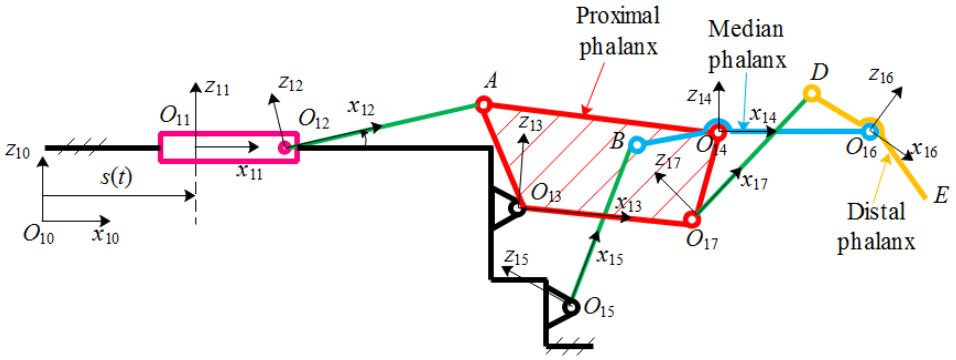

Fig. 6. Kinematic diagram of a finger

Subsystem $O_{11}O_{12}AO_{13}$ forms a slider-crank linkage mechanism.

The equation of motion of the linear motor which actuates slider 11 is

$$s(t) = v_0 t + x_0 , \tag{1}$$

where, for the thumb, v_0=-12.75 mm/s and x_0=36 mm, while for the other four fingers v_0=15 mm/s and x_0=61 mm. The v_0 values are maximal constructive limits of the linear servomotors for fingers 2-5, while for finger 1 it was chosen so that the geometrical limits are not exceeded during operation. The initial position parameters x_0 are also constructive dimensions of the servomotors.

Subsystems $O_{13}O_{14}BO_{15}$ and $O_{14}O_{16}DO_{17}$ form two other four-bar linkage mechanisms.

Calculations of the geometrical and kinematic parameters were performed starting from point O_1 and finishing with point E, while the dynamic parameters were determined afterward, in the opposite succession.

4. Positions of significant points of the hand-arm system

In the following, square matrices will be denoted by square brackets, while column ones by braces.

The positions of points O_i and E are determined using matrix transformations of the rotations about the axes of the corresponding joints,

$$\{X\}_j = [T]_{jk}\{X\}_k, \tag{2}$$

where:

- indexes j and k denote two arbitrary reference systems,
- system j is obtained by rotating system k first with angle φ about axis Ox, next with θ about Oy and finally with ψ about Oz;
- $\{X\}$ represents the coordinates column matrix,

$$\{X\} = \begin{Bmatrix} x \\ y \\ z \end{Bmatrix}, \tag{3}$$

- $[T]_{jk}$ is the rotation matrix between reference systems j and k [14], [15, p. 104], [16].

$$[T]_{ij} = \begin{bmatrix} c\theta \cdot c\psi & c\varphi \cdot s\psi + s\varphi \cdot s\theta \cdot c\psi & s\varphi \cdot s\psi - c\varphi \cdot s\theta \cdot c\psi \\ -c\theta \cdot s\psi & c\varphi \cdot c\psi - s\varphi \cdot s\theta \cdot s\psi & s\varphi \cdot c\psi + s\theta \cdot s\psi \\ s\theta & -s\varphi \cdot c\theta & c\varphi \cdot c\theta \end{bmatrix}, \tag{4}$$

- c and s before φ, θ and ψ denote cosine and sine, respectively of these angles.

The positions of points A, B, D and F result from the distances to joints O_{12} and O_{13}, O_{14} and O_{15}, O_{16} and O_{17}, as well as O_9 and O_{10}, respectively.

Thus, in the general case of two jointed bars, O_iP and O_jP, moving parallel to the plane Oxy (Fig. 7), the coordinates x and y of point P are determined from the system of equations

$$\begin{cases} \left(x-x_{O_i}\right)^2+\left(y-y_{O_i}\right)^2=O_iP^2 \\ \left(x-x_{O_j}\right)^2+\left(y-y_{O_j}\right)^2=O_jP^2. \end{cases} \tag{5}$$

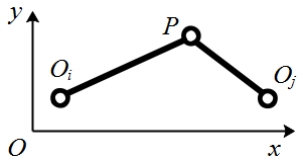

Fig. 7. System of two jointed bars

5. General formulae used in the kinematic analysis

To perform the kinematic analysis of the system, some general formulae were used.

For the general case of a Cartesian coordinate system, rotated as defined in Chapter 4, the column matrix of the components of the angular velocity vector is [15, p. 107], [16]:

$$\{\omega\}=\begin{bmatrix} \cos\theta\cdot\cos\psi & \sin\psi & 0 \\ -\cos\theta\cdot\sin\psi & \cos\psi & 0 \\ \sin\theta & 0 & 1 \end{bmatrix}\begin{Bmatrix} \dot{\varphi} \\ \dot{\theta} \\ \dot{\psi} \end{Bmatrix}. \tag{6}$$

The angular acceleration vector is:

$$\begin{Bmatrix} \varepsilon_x \\ \varepsilon_y \\ \varepsilon_z \end{Bmatrix}=\begin{Bmatrix} \dot{\omega}_x \\ \dot{\omega}_y \\ \dot{\omega}_z \end{Bmatrix}. \tag{7}$$

The composition formulae of the relative angular velocity and acceleration vectors, respectively, are [17, pp. 244, 250]

$$\overline{\omega}_{i,k}=\overline{\omega}_{i,j}+\overline{\omega}_{j,k}, \tag{8}$$

$$\overline{\varepsilon}_{i,k} = \overline{\varepsilon}_{i,j} + \overline{\varepsilon}_{j,k} + \overline{\omega}_{j,k} \times \overline{\omega}_{i,j}\,, \tag{9}$$

where an arbitrary notation $\overline{q}_{i,k}$ denotes the $\overline{q}$ vector quantity of reference system *i* in its motion with respect to reference system *k*.

The velocity and acceleration, respectively, of a point *P* of the reference system *i* with respect to the reference system *j* are [17, pp. 204, 205]:

$$\overline{v}_{P,j} = \overline{v}_{O_i,j} + \overline{\omega}_{i,j} \times \overline{O_iP}\,, \tag{10}$$

$$\overline{a}_{P,j} = \overline{a}_{O_i,j} + \overline{\varepsilon}_{i,j} \times \overline{O_iP} + \overline{\omega}_{i,j} \times \left(\overline{\omega}_{i,j} \times \overline{O_iP}\right). \tag{11}$$

The velocity and the acceleration of the point O_{11} of the slider are determined using the composition formulae known from the kinematics of the relative motion of a rigid body [17, pp. 244, 249],

$$\overline{v}_{O_{11},j} = \overline{v}_{O_{11},10} + \overline{v}_{O_{10},j} + \overline{\omega}_{10,j} \times \overline{O_{10}O_{11}}\,, \tag{12}$$

$$\overline{a}_{O_{11},j} = \overline{a}_{O_{11},10} + \overline{a}_{O_{10},j} + \overline{\varepsilon}_{10,j} \times \overline{O_{10}O_{11}} + \overline{\omega}_{10,j} \times \left(\overline{\omega}_{10,j} \times \overline{O_{10}O_{11}}\right) + 2\overline{\omega}_{10,j} \times \overline{v}_{O_{11},10}\,, \tag{13}$$

where the motion of the slider with respect to reference system 10 is a translation, hence

$$\overline{\omega}_{11,10} = 0\,, \tag{14}$$

$$\overline{\varepsilon}_{11,10} = 0\,. \tag{15}$$

In the general case of the jointed bars O_iP and O_jP in Figure 7, assuming that the velocities and accelerations of points O_i and O_j are known, the angular velocities and accelerations of the bars, as well as the velocity and acceleration of point *P*, are determined using formulae (10) and (11), respectively:

$$\overline{v}_P = \overline{v}_{O_i} + \overline{\omega}_i \times \overline{O_iP} = \overline{v}_{O_j} + \overline{\omega}_j \times \overline{O_jP}\,, \tag{16}$$

$$\overline{a}_P = \overline{a}_{O_i} + \overline{\varepsilon}_i \times \overline{O_iP} + \overline{\omega}_i \times \left(\overline{\omega}_i \times \overline{O_iP}\right) = \overline{a}_{O_j} + \overline{\varepsilon}_j \times \overline{O_jP} + \overline{\omega}_j \times \left(\overline{\omega}_j \times \overline{O_jP}\right). \tag{17}$$

6. General formulae used in the dynamic analysis

The theorem of linear momentum and the theorem of angular momentum with respect to the center of mass, applied to an arbitrary constituent body are,

$$m\bar{a}_C = \sum_i \bar{F}_i \,, \tag{18}$$

$$\bar{\bar{J}}_C \cdot \bar{\varepsilon} + \bar{\omega} \times \left(\bar{\bar{J}}_C \cdot \bar{\omega} \right) = \sum_j \bar{M}_j + \sum_i \bar{r}_i \times \bar{F}_i \,, \tag{19}$$

where the following notations were used:

- m - mass of the element;
- $\bar{a}_C$ - acceleration of the center of mass;
- $\bar{F}_i$ - forces acting upon the element;
- $\bar{\bar{J}}_C$ - tensor of inertia of the element with respect to its center of mass;
- $\bar{\omega}$ and $\bar{\varepsilon}$ - the absolute angular velocity and acceleration vectors, respectively;
- $\bar{M}_j$ - torques acting upon the element;
- $\bar{r}_i$ - position vector with respect to the center of mass of the application point of the force $\bar{F}_i$.

In matrix form, with respect to coordinate system k, equations (18) and (19) become

$$m\{a_C\}_k = \sum_i [T]_{ki} \{F_i\}_i \,, \tag{20}$$

$$[J_C]_k \{\varepsilon\}_k + [\hat{\omega}]_k [J_C]_k \{\omega\}_k = \sum_j [T]_{kj} \{M_j\}_j + \sum_i [T]_{ki} [\hat{r}_i]_i \{F_i\}_i \,, \tag{21}$$

respectively, where, for an arbitrary vector $\bar{w}$, the skew-symmetric matrix

$$[\hat{w}] = \begin{bmatrix} 0 & -w_z & w_y \\ w_z & 0 & -w_x \\ -w_y & w_x & 0 \end{bmatrix} \tag{22}$$

was introduced.

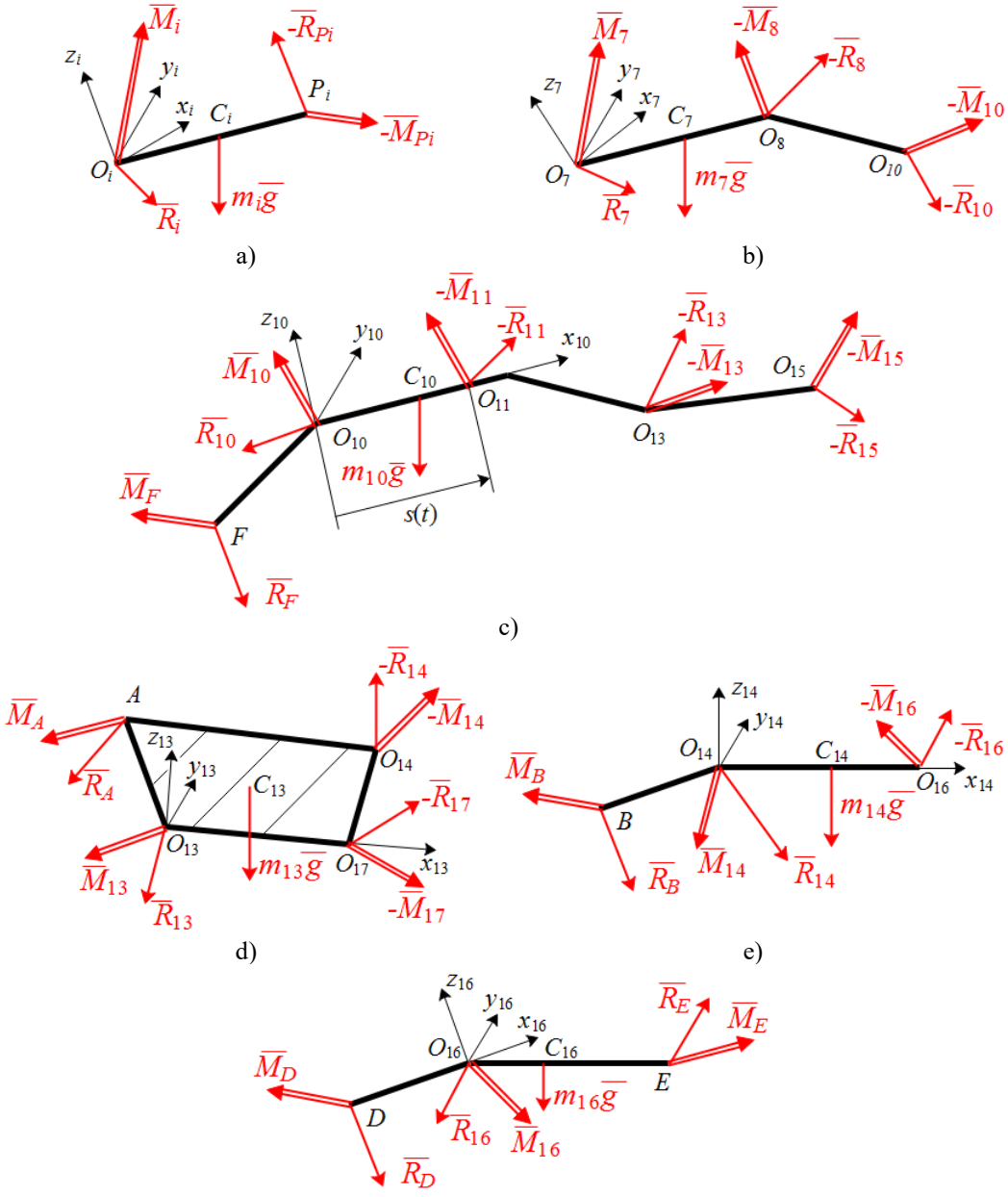

Fig. 8. The isolated elements of the hand-arm system

In Figure 8, the elements of the hand-arm system, considering an arbitrary finger, were isolated and the reaction forces and torques were represented, as follows:

- element i for i=1,…, 6, 8, 9, 11, 12, 15, 17 in Figure 8 a, where P_9=F, P_{12}=A, P_{15}=B, P_{17}=D, while P_i=O_{i+1} for the other values of i;

- elements 7, 10, 13, 14, 16 in Figures 8 b-f, respectively.

The linkages of the system are replaced by force and torque reactions, each with three components.

The minus sign of certain reactions was introduced to satisfy the action and reaction principle.

The system has the following active linkages:

- O_1,…, O_8 - revolute joints, where the torque components with respect to the rotation axes are the actuation torques;
- O_{11} - prismatic joint, with the position of the slider defined by equation (1), where the force component with respect to axis $O_{11}x_{11}$ is the actuation force.

All other linkages are passive. To avoid rigidly indeterminate unknowns, they were considered as follows:

- O_{10}, O_{13}, O_{14}, O_{16} - revolute joints (the torque components with respect to the rotation axes are null);
- O_9, O_{12}, O_{15}, O_{17} - universal joins, i.e. joints that obstruct the rotation about the torsion axis O_ix_i (the torque components with respect to O_iy_i and O_iz_i axes are null);
- F, A, B, D - spherical joints (all three components of the torque reactions are null).

Equations (20) and (21), written for all elements of the hand-arm assembly, form a linear algebraic system of 102 equations with 102 unknowns. The unknowns are the forces and torques in the joints (motor and reaction components).

The solving of this system is simplified by decoupling it into:

- 4 systems of 12 equations each, corresponding to subsystems O_9FO_{10}, $O_{12}AO_{13}$, $O_{14}BO_{15}$ and $O_{16}DO_{17}$, respectively;
- 9 systems of 6 equations each, corresponding to the bodies 1,…, 8 and 11.

7. Numerical application

A numerical application was considered, with the rotation angles of the arm elements and of the fingers (numbered according to Fig. 5 a), given in Tables 1 and 2, respectively.

Table 1

Rotation angles of the active joints of the robotic arm

Rotation angle	$\varphi_{0\text{-}1}$	$\theta_{1\text{-}2}$	$\varphi_{2\text{-}3}$	$\theta_{3\text{-}4}$	$\varphi_{4\text{-}5}$	$\psi_{5\text{-}6}$	$\theta_{6\text{-}7}$
Values	$0...\frac{\pi}{4}$	$\frac{\pi}{2}...\frac{3\pi}{4}$	$0...\frac{\pi}{4}$	$0...-\frac{\pi}{4}$	$0...-\frac{5\pi}{12}$	$0...\frac{\pi}{6}$	$0...-\frac{\pi}{6}$

Table 2

Rotation angle ψ_{7-8} for each finger

Finger	1	2	3	4	5
Values	$\frac{\pi}{10}...-\frac{\pi}{5}$	$\frac{\pi}{36}$	0	$-\frac{\pi}{60}$	$-\frac{\pi}{30}$

Each rotation angle varies in the time interval t_1=0…t_2=0.8s, according to a law of motion which was chosen so that the motion starts and ends with null relative angular velocities and accelerations. Such a law of motion should be expressed by a function with null first and second-order derivatives, at the initial and final moments of time, t_1 and t_2, respectively. Considering the initial and the final value of an arbitrary rotation angle, f_1 and f_2, respectively, the following expression of the function was obtained [18] (Fig. 9):

$$f(t)=f_1+(f_2-f_1)\cdot\left(\frac{t-t_1}{t_2-t_1}-\frac{\sin 2\pi\frac{t-t_1}{t_2-t_1}}{2\pi}\right). \tag{23}$$

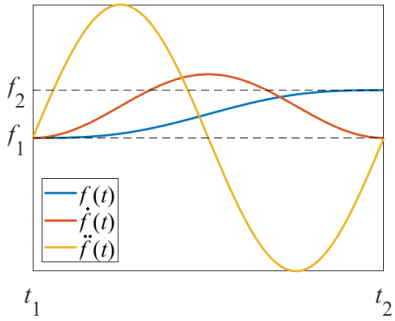

Fig. 9. Shape of the law of motion and its derivatives, for an arbitrary rotation angle

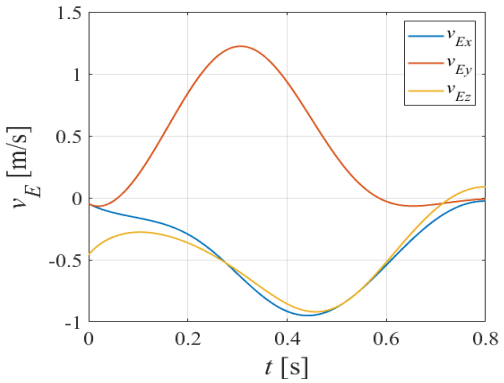

Fig. 10. Velocity components of the thumb tip

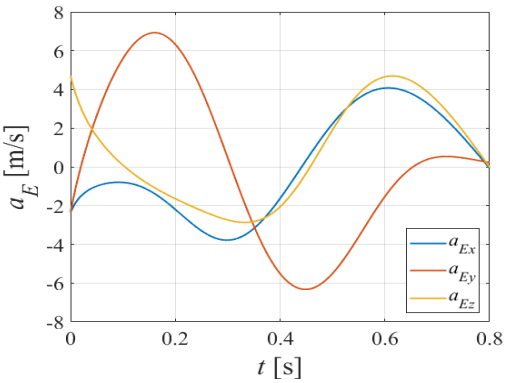

Fig. 11. Acceleration components of the thumb tip

Figures 10 and 11 display the variations of the velocity and acceleration components of the tip of the thumb (finger 1), obtained by kinematic analysis.

The mass and the matrix of inertia of each element were determined from the 3D model created by the authors in CATIA V5 CAD program.

To determine the time variations of the motor and reaction forces and torques in the joints, for the given motion defined above, an original MATLAB program has been developed to solve the systems presented in Chapter 6. The system was solved for a discrete set of values chosen in the time interval $t_1 \ldots t_2$, with the step Δt=0.001s.

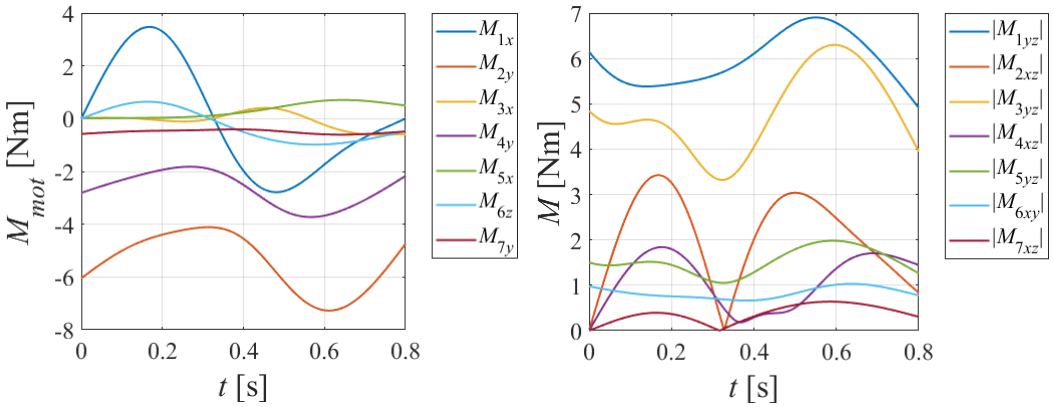

a) Motor components b) Magnitudes of the reaction components

Fig. 12. Torques in the joints of the robotic arm

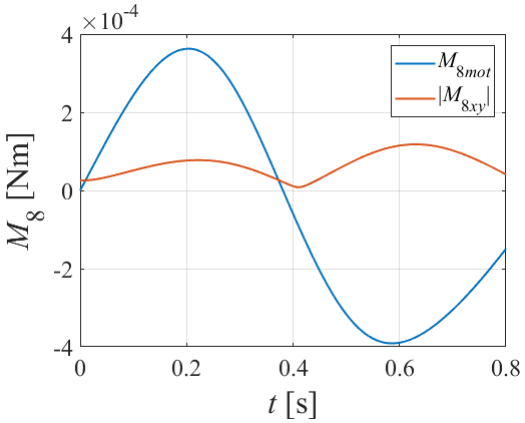

Fig. 13. Motor (M_{8mot}) and reaction (M_{8xy}) torque in joint 8, for finger 1

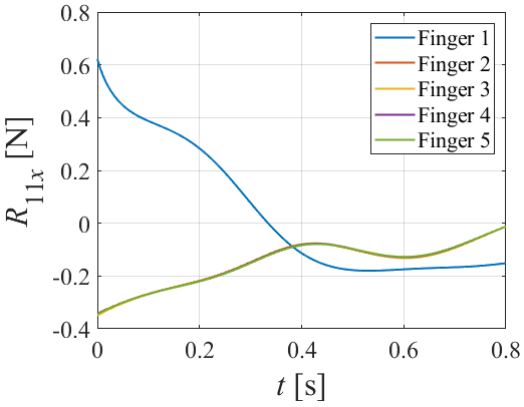

Fig. 14. Motor force in slider 11

In Figure 12, the variations of the torques in the joints of the robotic arm are displayed (a - motor components, i.e. torque components along the rotation axes; b - magnitudes of the reaction components, i.e. torque components normal to the rotation axes).

Figure 13 displays the variations of the motor component and the reaction component, respectively, of the torque in joint 8 of finger 1.

In Figure 14 the motor forces in the sliders are displayed, distinct for finger 1 and, because of their almost identical geometry, indistinct for fingers 2-5.

The results were successfully verified by applying the theorem of linear momentum, and of angular momentum with respect to point O_1, for certain subsystems, such as $O_{14}O_{16}DO_{17}$, $O_{13}O_{14}BO_{15}$, $O_{11}O_{12}AO_{13}$, $O_{10}\ldots O_{17}$, $O_1\ldots O_{17}$.

9. Conclusions

The used grasping device is a mechanism with a reduced number of mobilities, compared to a human hand, which makes it cheaper, lighter and easier to build than a more realistic model.

To improve the functionality of the existing commercial hand, a supplementary mobility of the thumb was introduced.

Due to their simplicity and relatively small sizes, most parts of the device are suited for manufacturing by 3D printing. Furthermore, improvements can be easily brought.

The study presents a complete direct kinematic and dynamic analysis of the device.

In the chosen configuration, the necessary motor torque of the servomotor in joint 2 is the highest, which is explained by the large arms of the component weights, with respect to point O_2. This outcome leads to the need for either a powerful enough actuator or the decrease of the required torque, using a counterweight system or a system of elastic elements.

The reaction torques in joints 1 and 3 are considerably higher than the others, therefore a stiffer design of the corresponding parts is necessary.

The small values of the components of torque M_8 are due to the small values of the inertial parameters of the finger 1, as well as of the length O_8O_9.

The results provide useful calculation data for the basic design of a hand-arm robotic system, as well as for an optimization process.

REFERENCES

[1]. *D. Choi, D.-W. Lee, W. Shon and H.-G. Lee,* "Design of 5 D.O.F Robot Hand with an Artificial Skin for an Android Robot", in The Future of Humanoid Robots - Research and Applications, InTech, Rijeka, Croatia, pp. 81–96, 2012.

[2]. *R.M. Murray, Z. Li, S. Sastry,* "A mathematical introduction to robotic manipulation", CRC Press Inc., Boca Raton/U.S.A., 2006.

[3]. F. *Touvet, N. Daoud, J.P. Gazeau, S. Zeghloul, M.A. Maier and S. Eskiizmirliler*, "A biomimetic reach and grasp approach for mechanical hands", in Journal of Robotics and Autonomous Systems, **vol. 60**, no. 3, 2012, pp 473-486.

[4]. *K. Abdel-Malek, J. Yang, T. Marler, S. Beck, A. Mathai, X. Zhou, A. Patrik and J. Arora*, "Towards a new generation of virtual humans", in International Journal of Human Factors Modelling and Simulation, **vol. 3**, no. 1, 2006, pp 2-39.

[5]. *A.V. Săvescu, L. Cheze, W. Xuguang, G. Beurier and J.P. Verriest,* "A 25° of freedom hand geometrical model for better hand attitude simulation", in SAE transactions, **vol. 113**, no. 1, 2004, pp 270-275.

[6]. *H. Kawasaki, T. Komatsu, K. Uchiyama and T. Kurimoto,* "Dexterous anthropomorphic robot hand with distributed tactile sensor: Gifu hand II", in IEEE International Conference on Systems, Man, and Cybernetics Proceedings, **vol. 2**, pp. 782-787, 1999.

[7]. *R. Mahmoud, A. Ueno and S. Tatsumi*, "Dexterous Mechanism Design for an Anthropomorphic artificial hand: Osaka City University Hand I," in 10th IEEERAS International Conference on Humanoid Robots, Nashville, TN, 2010.

[8]. *H. Park and D. Kim*, "An open-source anthropomorphic robot hand system: HRI hand" in HardwareX, **vol. 7**, 2020

[9]. *A. Nurpeissova, T. Tursynbekov and Almas Shintemirov*, "An Open-Source Mechanical Design of ALARIS Hand: A 6-DOF Anthropomorphic Robotic Hand" in Proceedings of the 2021 IEEE International Conference on Robotics and Automation (ICRA 2021), Xi'an, China, 2021, pp. 1077-1183.

[10]. https://www.rmigo.com/shop/platforms/arduino/lobot-uhand-arduino-gestrure-recognition-bionic-mechanical-hand/

[11]. https://uk.banggood.com/LOBOT-uHand-STM32-Open-Source-RC-Robot-Right-Arm-APP-or-Stick-or-Glove-Control-Educational-Robot-Arm-Kit-p-1403202.html?cur_warehouse=CN

[12]. *M. Ionescu, I. Borcoşi, Gh. Gîlcă and N.G. Bîzdoacă*, "Description and control of a Lobot uHand STM 32 structure" in Annals of the „Constantin Brancusi" University of Târgu Jiu, Engineering Series, no. 1, Târgu Jiu, Romania, 2019, pp. 14-19.

[13]. *M. Ionescu, Gh. Gîlcă, I. Borcoşi, F.L. Besnea (Petcu), S.I. Cismaru and N.G. Bîzdoacă*, "The Simulation of positioning of a Lobot uHand STM32 structure" in 2019 International Conference on Electromechanical and Energy Systems (SIELMEN), Craiova, Romania, 2019, pp. 1-6.

[14]. *Şt. Dumitru and A. Craifaleanu*, "Kinematic model of an anthropomorphic robotic arm" in Annals of Faculty Engineering Hunedoara, International Journal of Engineering, **vol. 20**, no. 1, Hunedoara, Romania, 2022, pp. 55-60.

[15]. *L.A. Pars*, A Treatise on Analytical Dynamics, Heinemann Educational Books Ltd, London, 1965.

[16]. *I. Stroe, S. Staicu and A. Craifaleanu*, "Internal forces calculus of compass robotic arm using Lagrange equations" in 10th ESA Workshop on Advanced Space Technologies for Robotics and Automation 'ASTRA 2011', at ESTEC, Noordwijk, (on CD-ROM), 2011, pp. 1-6.

[17]. *R. Voinea, D. Voiculescu and V. Ceauşu*, Mecanica (Mechanics), Editura didactică şi pedagogică, Bucureşti, 1983.

[18]. https://math.stackexchange.com/questions/569856/function-with-zero-first-to-nth-derivative-at-end-points.

Appendix. Numeric data

Table 3

Geometry with respect to body reference systems $O_{ix_iy_iz_i}$

i	Finger	O_iC_{ix} [mm]	O_iC_{iy} [mm]	O_iC_{iz} [mm]	P	C_iP_x [mm]	C_iP_y [mm]	C_iP_z [mm]
1	-	374.1	14.9	-1.9	O_2	94.9	-14.9	-8.1
2	-	75.1	0.2	-8	O_3	53.4	-0.2	8
3	-	186.4	15.1	7.2	O_4	50.6	-15.1	7.2
4	-	110.7	0.2	-6.7	O_5	72.7	-0.2	6.8
5	-	69.7	-10.4	-20.7	O_6	12.3	10.4	20.7
6	-	58.3	19.9	-9.6	O_7	14.7	-19.9	9.6
7	1	110.5	-0.1	0.3	O_8	-26.5	10	6
	2					-42	25.3	23.6
	3					9.3	11	23.6
	4					-31.4	-3.7	23.6
	5					-29.5	-23	23.6
	1	110.5	-0.1	0.3	O_{10}	55.4	13	-5.4
	2-5					0	0	0
8	1	0	0	-3	O_9	6.9	-0.1	4.7
	2-5	0	0	0		0	0	0
9	1	29.2	0	1	F	29.9	0	-1
	2-5	0	0	0		0	0	0
10	1	-35.7	-0.2	-19.4	F	-42.7	0.3	32.4
					O_{11}	$s(t)$	-0.5	-4.1
					O_{13}	72.6	1	3.9
					O_{15}	79.8	-5.6	24.7
	2	0	0	0	F	0	0	0
					O_{11}	$s(t)$	0	0
					O_{13}	153	-7.3	-12.4
					O_{15}	160	-13.9	-33.3
	3	0	0	0	F	0	0	0
					O_{11}	$s(t)$	0	0
					O_{13}	114	-0.9	-12.4
					O_{15}	121	-7.5	-33.3
	4	0	0	0	F	0	0	0
					O_{11}	$s(t)$	0	0
					O_{13}	146	0.9	-12.4
					O_{15}	153	-5.8	-33.3
	5	0	0	0	F	0	0	0
					O_{11}	$s(t)$	0	0
					O_{13}	138	7.3	-12.4
					O_{15}	145	0.7	-33.3
11	1	0	0	0	O_{12}	14.3	-3.1	0
	2					14.3	-4.1	0
	3					14.3	-3.1	0
	4					14.3	3.1	0
	5					14.3	4.1	0
12	1	14.9	-1	0	A	13.1	1	0
	2	34.8	0	0		33.9	0	0
	3	15.2	-1	0		14.6	1	0
	4	31.3	1	0		30.4	0	0
	5	27.3	0	0		26.4	0	0

13	1	14.4	0	3.7	*A*	-6.2	-4.5	-9.9
					O_{14}	15.2	-2.2	3.5
					O_{17}	17	2.2	-3.7
	2-5	18.8	0	7	*A*	-26.9	3.2	-5.1
					O_{14}	24.5	-2.2	1
					O_{17}	24.7	2.2	-7
14	1	11.6	-2.2	-0.1	*B*	-10.6	-2.2	-9.9
					O_{16}	17.4	2.2	0.1
	2-5	13.2	-2.2	0.1	*B*	-27.2	-2.2	-0.1
					O_{16}	24.8	2.2	-0.1
15	1	16.8	-0.5	5.5	*B*	24.5	0.5	-5.5
	2-5	18.3	-0.5	-2		19.2	0.5	2
16	1	6.1	2.2	4	*D*	-14.6	2.2	-4
					E	12.3	0	-1
	2-5	7.3	2.2	3.4	*D*	-15.3	2.2	-3.4
					E	11.5	0	-0.9
17	1	12.2	0.5	1.1	D	12.2	-1.5	-1.1
	2-5	16.5	0.5	1.3		16.5	-0.5	-1.3

Table 4

Inertial parameters with respect to central reference systems $C_ix_iy_iz_i$

Body	Finger	*m* [g]	J_x [kg·m^2]	J_y [kg·m^2]	J_z [kg·m^2]	J_{xy} [kg·m^2]	J_{yz} [kg·m^2]	J_{zx} [kg·m^2]
1	-	137	$9.143\cdot10^{-5}$	0.003	0.003	$1.69\cdot10^{-4}$	$-1.577\cdot10^{-5}$	$-2.176\cdot10^{-5}$
2	-	81	$2.337\cdot10^{-5}$	$1.331\cdot10^{-4}$	$1.175\cdot10^{-4}$	$-1.326\cdot10^{-6}$	$1.418\cdot10^{-7}$	$-1.397\cdot10^{-5}$
3	-	136	$1.060\cdot10^{-4}$	$7.039\cdot10^{-4}$	$7.546\cdot10^{-4}$	$1.03\cdot10^{-4}$	$1.017\cdot10^{-5}$	$4.368\cdot10^{-5}$
4	-	97	$2.435\cdot10^{-5}$	$3.340\cdot10^{-4}$	$3.175\cdot10^{-4}$	$-1.957\cdot10^{-6}$	$1.195\cdot10^{-7}$	$-2.658\cdot10^{-5}$
5	-	99	$9.175\cdot10^{-5}$	$1.027\cdot10^{-4}$	$6.093\cdot10^{-5}$	$-6.712\cdot10^{-6}$	$6.058\cdot10^{-6}$	$-2.444\cdot10^{-5}$
6	-	103	$9.483\cdot10^{-5}$	$7.728\cdot10^{-5}$	$1.200\cdot10^{-4}$	$2.942\cdot10^{-5}$	$-5.213\cdot10^{-6}$	$-7.627\cdot10^{-6}$
7	-	364	$4.479\cdot10^{-4}$	0.001	0.001	$4.164\cdot10^{-6}$	$7.516\cdot10^{-6}$	$3.18\cdot10^{-5}$
8	1	1.03	$2.503\cdot10^{-8}$	$2.503\cdot10^{-8}$	$4.191\cdot10^{-8}$	$-2.482\cdot10^{-24}$	0	0
	2-5	0	0	0	0	0	0	0
9	1	0.75	$4.961\cdot10^{-8}$	$3.731\cdot10^{-7}$	$3.260\cdot10^{-7}$	$-3.223\cdot10^{-12}$	$4.298\cdot10^{-10}$	$-3.593\cdot10^{-12}$
	2-5	0	0	0	0	0	0	0
10	1	35	$5.327\cdot10^{-6}$	$5.322\cdot10^{-5}$	$4.947\cdot10^{-5}$	$3.605\cdot10^{-7}$	$1.718\cdot10^{-7}$	$5.492\cdot10^{-6}$
	2-5	0	0	0	0	0	0	0
11	1-5	6	$2.103\cdot10^{-8}$	$2.181\cdot10^{-7}$	$2.167\cdot10^{-7}$	0	$-3.882\cdot10^{-22}$	$-1.209\cdot10^{-22}$
12	1	0.57	$2.302\cdot10^{-8}$	$7.224\cdot10^{-8}$	$5.035\cdot10^{-8}$	$3.242\cdot10^{-10}$	$-2.703\cdot10^{-12}$	$1.881\cdot10^{-10}$
	2	0.79	$1.903\cdot10^{-9}$	$4.843\cdot10^{-7}$	$4.833\cdot10^{-7}$	$1.790\cdot10^{-13}$	$-4.030\cdot10^{-20}$	$-8.950\cdot10^{-14}$
	3	0.56	$1.816\cdot10^{-9}$	$5.452\cdot10^{-8}$	$5.358\cdot10^{-8}$	$4.397\cdot10^{-14}$	$-4.194\cdot10^{-20}$	$-2.940\cdot10^{-14}$
	4	0.75	$1.888\cdot10^{-9}$	$3.678\cdot10^{-7}$	$3.668\cdot10^{-7}$	$1.547\cdot10^{-13}$	$-4.061\cdot10^{-20}$	$-7.872\cdot10^{-14}$
	5	0.71	$1.870\cdot10^{-9}$	$2.572\cdot10^{-7}$	$2.562\cdot10^{-7}$	$1.269\cdot10^{-13}$	$-4.102\cdot10^{-20}$	$-6.639\cdot10^{-14}$
13	1	2.30	$1.001\cdot10^{-5}$	$5.996\cdot10^{-6}$	$5.465\cdot10^{-6}$	$-1.308\cdot10^{-6}$	$4.915\cdot10^{-6}$	$-1.566\cdot10^{-6}$
	2-5	2.64	$7.606\cdot10^{-7}$	$2\cdot10^{-6}$	$1.248\cdot10^{-6}$	$7.957\cdot10^{-20}$	$1.173\cdot10^{-19}$	$4.92\cdot10^{-7}$
14	1	1.85	$4.495\cdot10^{-8}$	$3.466\cdot10^{-7}$	$3.076\cdot10^{-7}$	$-8.013\cdot10^{-22}$	$-4.196\cdot10^{-22}$	$4.981\cdot10^{-9}$
	2-5	1.71	$2.191\cdot10^{-8}$	$4.36\cdot10^{-7}$	$4.196\cdot10^{-7}$	0	$6.617\cdot10^{-24}$	$-7.127\cdot10^{-10}$
15	1	0.96	$4.918\cdot10^{-8}$	$2.902\cdot10^{-7}$	$2.412\cdot10^{-7}$	$4.125\cdot10^{-22}$	$3.970\cdot10^{-23}$	$-5.576\cdot10^{-8}$
	2-5	0.80	$1.554\cdot10^{-8}$	$1.511\cdot10^{-7}$	$1.356\cdot10^{-7}$	0	0	$-1.753\cdot10^{-8}$
16	1	0.96	$2.110\cdot10^{-8}$	$8.638\cdot10^{-8}$	$6.836\cdot10^{-8}$	$2.210\cdot10^{-22}$	$1.278\cdot10^{-23}$	$2.265\cdot10^{-8}$
	2-5	0.88	$1.603\cdot10^{-8}$	$8.587\cdot10^{-8}$	$7.267\cdot10^{-8}$	$4.938\cdot10^{-23}$	$-1.937\cdot10^{-23}$	$-2.122\cdot10^{-8}$
17	1	0.50	$2.283\cdot10^{-9}$	$4.859\cdot10^{-8}$	$4.639\cdot10^{-8}$	$-6.885\cdot10^{-24}$	$3.647\cdot10^{-25}$	$-5.111\cdot10^{-18}$
	2-5	0.62	$2.745\cdot10^{-9}$	$9.543\cdot10^{-8}$	$9.279\cdot10^{-8}$	0	0	$-6.617\cdot10^{-24}$